Journal of Environmental Chemical Engineering 11 (2023) 109186

Contents lists available at ScienceDirect

Journal of Environmental Chemical Engineering

journal homepage: www.elsevier.com/locate/jece

Efficient degradation of triclosan by aluminium acetylacetonate doped polymeric carbon nitride photocatalyst under visible light

Danyan Sun [a,b], Xiaohu Lin [a,c], Jingcheng Xu [a], Zhibo Lu [a], Juwen Huang [a], Shiyi Li [c], Luiza C. Campos [b,*]

[a] State Key Laboratory of Pollution Control and Resource Reuse, Key Laboratory of Yangtze Water Environment, Ministry of Education, College of Environmental Science and Engineering, Tongji University, Shanghai 200092, China
[b] Department of Civil, Environmental and Geomatic Engineering, University College London, Gower Street, London WC1E 6BT, United Kingdom
[c] PowerChina Huadong Engineering Corporation Limited, Hangzhou 311122, China

ARTICLE INFO

Editor: Luigi Rizzo

Keywords:
Photocatalytic degradation
Triclosan
Visible light
Polymeric carbon nitride
Aluminium acetylacetonate
Degradation pathway

ABSTRACT

Triclosan (TCS), as a typical toxic and harmful micro-pollutant, has been frequently detected in various water bodies, and its threat to the aquatic environment has raised significant concerns. In this study, aluminium acetylacetonate doped polymeric carbon nitride photocatalysts (PCN-AA) were synthesized to investigate the degradation properties of TCS under simulated visible light. The results showed that the best ratio material PCN-AA30 ($k = 0.0529\ min^{-1}$) can degrade 99.29 % of TCS in 90 min, which is 2.45 times the degradation of the original polymeric carbon nitride material PCN-AA0 ($k = 0.0216\ min^{-1}$). The degradation process of TCS presented different rules under the changing conditions of catalyst dosage, initial concentration of TCS, pH, common inorganic anions and natural organic matter in water. The results of radicals quencher experiment showed that $\cdot O_2$ played the most important role in the photocatalytic degradation in the reaction system. This study also identified 10 degradation products of TCS using UPLC-Q-TOF technology and proposed the possible degradation pathways. In addition, the acute biotoxicity of PCN-AA materials were tested by luminescent bacteria method, indicating that the safety of PCN-AA was relatively high. These results demonstrated that the polymeric carbon nitride material doped with aluminium acetylacetonate is a promising catalyst for the degradation of micro-pollutants in water under visible light.

1. Introduction

With the excessive use of various chemicals and the rapid development of water environment analysis and detection technology, micro-pollutants represented by pharmaceuticals and personal care products (PPCPs), endocrine disruptors (EDCs), persistent organic pollutants (POPs) and disinfection byproducts (DBPs) are frequently detected in the aquatic environment [1]. Although concentrations of these pollutants are in the lower range (μg L^{-1} or even ng L^{-1}), their persistence and toxicity could not be ignored [2]. TCS is one of the typical PPCPs which is widely used as a broad-spectrum antibacterial agent in personal care products such as household cleaners, shower gels, soaps and toothpastes [3,4]. More than 96 % of TCS enters the sewer systems and ends up in the environment under normal use [5]. In recent years, many studies have reported the detection of TCS in surface water and water reuse systems. For example, the concentration of TCS in surface water was found to be 10.9–241 ng L^{-1} [6], the average concentration in natural watershed was 7.5 ng L^{-1} [7], and the concentration in receiving river replenished with reclaimed water was 61–660 ng L^{-1} [8]. Even if the concentration level of TCS is very low, it may still exhibit relatively high acute or chronic toxicity to aquatic organisms, or even threaten the human health, such as endocrine disruption and reproductive problems [9–11]. Therefore, it is necessary to take certain measures to effectively prevent the release of these micro-pollutants in the water environment and reduce their potential ecological and health risks.

The conventional sewage treatment processes are usually only aimed at the further removal of general pollutants, but lack of efficient and targeted removal of micro-pollutants. As a result, a large number of micro-pollutants that are difficult to degrade will be released into environmental water bodies through wastewater treatment plants. Currently, many scholars have carried out researches on the degradation of micro-pollutants in water using advanced oxidation processes (AOP)

* Corresponding author.
E-mail address: l.campos@ucl.ac.uk (L.C. Campos).

https://doi.org/10.1016/j.jece.2022.109186
Received 16 September 2022; Received in revised form 15 December 2022; Accepted 16 December 2022
Available online 19 December 2022

such as Fenton oxidation, photocatalysis and electrochemical oxidation [12–15]. Compared with traditional treatment technologies such as adsorption and membrane treatment, AOP has a better effect on micro-pollutants degradation, and has the advantages of low selectivity and no secondary pollution [16]. It showed great application potential for the removal of micro-pollutants from water. And photocatalytic oxidation technology is widely used due to its obvious advantages in energy consumption, economy and high efficiency [17]. Photocatalytic materials can generate photogenerated electron-hole pairs when excited by ultraviolet (UV) light or visible light. Such electron-hole pairs will form a series of active species (·OH, $\cdot O_2^-$, etc.) during the reaction process, and then degrade the target pollutants by destroying the bond energy structure [18]. At present, the photocatalysts that are more researched include WO_3 [19], $BiVO_4$ [20], TiO_2 [21], polymeric carbon nitride (PCN) [22] and graphene (rGO) [23], and the polymeric carbon nitride has become one of the most commonly used ideal photocatalytic materials due to its good band gap, low cost and environmental friendliness, such as the degradation of organic pollutants and hydrogen production [24,25]. However, unmodified PCN has poor photocatalytic performance due to the insufficient visible light absorption and high recombination rate of photogenerated charge carriers [26]. Therefore, many studies have taken various approaches to prepare modified PCN materials to improve the photocatalytic efficiency, including the construction of heterogeneous structures [27], element doping [28], molecular copolymerization [29] and noble metal deposition [30].

Most of the current researches on the photocatalytic degradation of TCS are under UV light irradiation [31–33], and there are relatively few experimental studies using the visible light reaction system. And the improved polymeric carbon nitride materials could show a larger visible light response range and excellent photocatalytic activity. For example, Yang et al. (2020) controlled the electronic structure of PCN by in situ keto-enol cyclization of urea and acetylacetone, which effectively enhanced the visible light absorption and photocatalytic efficiency [34]. On this basis, Choi et al. (2018) introduced the bidentate metal coordination site of Al element in acetylacetonate doped polymeric carbon nitride, which further changed the photocatalytic performance, improved the activity of photocatalytic degradation and had the advantages of relatively simple preparation process and low cost [35]. However, most of the researches related to modified PCN only focused on the synthesis and properties of materials, rather than the specific and applied analysis of the micro-pollutant degradation using photocatalytic materials. Therefore, the aim of this work was to investigate the degradation of TCS by modified PCN materials in detail. This is the first time aluminium acetylacetonate ($Al(aa)_3$) doped PCN photocatalytic material is applied to degrade TCS under visible light conditions. First, the morphology, structure and optical properties of the material samples were analysed by characterization methods, and then the photocatalytic degradation rules of TCS under different reaction conditions or influencing factors were analysed specifically. Through the radicals quencher experiment, electron paramagnetic resonance and UPLC-Q-TOF techniques, the degradation mechanisms and pathways of TCS were explored. Finally, the safety and applicability of the photocatalytic materials were investigated by the luminescent bacteria acute toxicity test. This work systematically studied the degradation behaviour of TCS by PCN based photocatalysts, which may provide valuable insights for the engineering application of efficient micro-pollutants degradation by improved polymeric carbon nitride materials under visible light.

2. Materials and methods

2.1. Materials and reagents

All chemicals were used directly without further purification, and ultrapure water was used in all experiments. The details can be seen in Table S1 (Supplementary Material).

2.2. Preparation of photocatalytic materials

The preparation of photocatalytic materials was referred to Choi et al. and Zhou et al. [35,36]. 10 g of urea and aluminium acetylacetonate (0.005 g, 0.01 g, 0.02 g and 0.03 g) were ground for 5 min to achieve complete uniformity and then placed in the alumina crucible with a cover. The mixed solids were heated at 3.6 °C min^{-1} to 550 °C in a muffle furnace (150 min) and maintained for 2 h in air. After the reactions were completed and cooled to the ambient temperature, the obtained products were taken out of the furnace and exfoliated in an ultrasonic bath (200 W) for 10 min, and filtered with the 0.22 μm pore size microporous membrane (aqueous). Finally, after washing repeatedly with deionized water, the products were dried under vacuum at 60 °C for 6 h. The final form of the PCN-AA materials was powder.

The material samples were labelled as PCN-AA5, PCN-AA10, PCN-AA20 and PCN-AA30, containing 0.005 g, 0.01 g, 0.02 g and 0.03 g of $Al(aa)_3$, respectively. For comparison, original PCN-AA0 material was prepared without the addition of $Al(aa)_3$, only obtained by the thermal decomposition and polymerization of urea.

2.3. Characterization

Powder X-ray diffraction (XRD) was done by using X-ray diffractometer (Bruker D8 Advance) with Cu-Kα radiation ($\lambda = 1.5406$ Å) at 40 kV and 40 mA in the scan range of $2\theta = 10–80°$. Fourier transformed infrared (FT-IR) spectra were recorded by Thermo Scientific Nicolet iS5 in the range of 400–4000 cm^{-1} and were carried out by KBr tablet method. Scanning electron microscope (SEM, ZEISS Gemini 300) and transmission electron microscope (TEM, JEOL JEM 2100F) were used to analyse the surface microstructure and morphology, and the element mapping was carried out by energy dispersive x-ray spectrometer (EDX, OXFORD Xplore) equipped with SEM. Brunauer-Emmett-Teller (BET) specific surface area was measured by automatic specific surface area analyser (Mack ASAP2460) and the adsorbate gas was N_2. The quantitative determination of Al element was analysed on inductively coupled plasma mass spectrometer (ICP-MS, Aglient 780). The chemical states such as surface valence was investigated by X-ray photoelectron spectroscopy (XPS, Thermo Scientific K-Alpha) with Al Kα X-ray, and the binding energy was calibrated with C 1s = 284.80 eV as standard. Light absorption properties were analysed by Ultraviolet-visible diffuse reflectance spectra (UV-Vis, Shimadzu UV-3600) with standard BaSO4 powder as the reference standard, the test range was 300–700 nm. Photoluminescence spectra (PL, Edinburgh FLS1000) were reflected in the range of 300–800 nm with an excitation wavelength of 365 nm. The reactive free radicals were measured by electron paramagnetic resonance spectrometer (EPR, Bruker EMXPLUS).

2.4. Degradation experiment of TCS under visible light

The photocatalytic degradation experiments used a xenon lamp (500 W) and 400 nm filters to simulate visible light irradiation conditions in the photochemical reactor (Fig. S1). 10 mg of the photocatalytic materials were uniformly dispersed in 50 mL of TCS solution with the initial concentration of 2 mg L^{-1} (except in the experiments on the influence of catalyst dosages and initial concentrations of TCS). In order to reach the adsorption-desorption balance of TCS on the surface of the photocatalytic material, the reaction system was placed in the dark for 30 min under magnetic stirring at 500 rpm before turning on the xenon lamp and the photochemical reactor device. The photocatalytic degradation process took 120 min, and 1 mL of samples were taken at 0, 10, 20, 30, 50, 70, 90, and 120 min respectively (0 min means that the dark adsorption was over and the photocatalytic reaction began), and then filtered with a 0.22 μm filter for subsequent analysis. Parallel experiments and blank control were set up in each group.

2.5. Analysis of TCS

The concentration of TCS was determined by high performance liquid chromatography-diode array detector (HPLC-DAD, Angilent 1200), using a GL Science Inertsil ODS-SP column (250 mm × 4.6 mm, 5 μm). The test conditions were: isocratic elution, the ratio of mobile phase A (ultrapure water with 0.1 % formic acid) to mobile phase B (acetonitrile) was 20:80, mobile phase flow rate was 1.0 mL min^{-1}, column temperature maintained at 30 °C, detection wavelength was 282 nm, injection volume was 50 μL, and test time was 7 min. The calibration range was from 50 to 5000 μg L^{-1}. These conditions resulted in a linear response, with R^2 (correlation coefficient) of 0.99, limits of detection (LOD) of 50 μg L^{-1} and limits of quantification (LOQ) of 500 μg L^{-1}.

The degradation products of TCS were analysed by ultra-performance liquid chromatography-quadrupole time-of-flight mass spectrometer (UPLC-Q-TOF), and using a Waters HSS T3 column (3.0 × 100 mm, 1.7 μm). The test conditions were: mobile phases were 0.05 % formic acid (phase A) and acetonitrile (phase B), flow rate was 0.3 mL min^{-1}, injection volume was 5.0 μL. The negative ion scanning mode (ESI-) was used to collect signals from 50 to 1200 m z^{-1}, and the liquid phase gradient elution settings during the analysis were shown in Table S2. External calibration of UPLC-Q-TOF with the sodium formate solution was performed before each injection.

2.6. Luminescent bacteria toxicity test

The safety assessment of the PCN-AA in water was determined by the luminescent bacteria method. The relative luminosity of luminescent bacteria was shown to have a significantly negative correlation with the total concentration of toxic components in the water sample ($p \leq 0.05$). At the same time, the luminescent inhibition ratio was significantly positively correlated with the total concentration of toxic components [37]. So, the acute toxicity level can be expressed by measuring the relative luminosity, and luminescent inhibition ratio can be calculated by the following equation:

$$\text{Luminescent inhibition ratio (\%)} = 100\ \% - \text{relative luminosity (\%)} \quad (1)$$

The test method of luminescent inhibition ratio referred to Water Quality-Determination of the acute toxicity-Luminescent bacteria test (GB/T 15441–1995) [38], and the test instrument is the biological toxicity tester (DXY-3). The acute toxicity grade divided by the luminescent inhibition ratio referred to the percentage grade score standard which was recommended by Nanjing Institute of Soil Science, Chinese Academy of Sciences (Table S3).

3. Results and discussion

3.1. Characterization of PCN-AA

3.1.1. Structure and morphology

The XRD patterns of PCN-AA photocatalytic materials with different ratios are shown in Fig. 1(a). There were two diffraction peaks at 2θ = 12.9° and 2θ = 27.5° in the diffractogram, compared with the standard card of PCN (JCPDS87–1526); and these two characteristic peaks corresponded to the (100) and (002) crystal plane, respectively. The diffraction peak at 12.9° was ascribed to the in-plane packing of tri-s-triazine units (100), and the peak at 27.5° was ascribed to the stacking of conjugated aromatic planes (002) [39]. With the increase of Al $(aa)_3$ addition during the material preparation, two characteristic peaks were gradually weakened and broadened, indicating that the planar structure of carbon nitride was distorted to varying degrees at the Al coordination centre [35]. Meanwhile, no obvious peak shift could be observed in Fig. 1(a), so there was no change in the basic structure of the PCN.

The FT-IR spectra results of the PCN-AA with different ratios are shown in Fig. 1(b). The broad band at 3000–3300 cm^{-1} in the FT-IR spectra was corresponded to the stretching vibration of the N-H bond; the characteristic peaks in the range from 1100 to1800 cm^{-1} were attributed to the stretching vibration mode of CN heterocycles; the peak at 810 cm^{-1} was related to the bending vibration of triazine units in the structure of PCN [26,27,36]. In addition, since the doping of $Al(aa)_3$ during the preparation of PCN photocatalytic materials, the characteristic peaks of each material gradually became less sharp, but were still similar to the original PCN-AA0, again indicating that the typical structure of polymeric carbon nitride in PCN-AA did not change significantly.

The PCN-AA materials were analysed by ICP-MS to determine the content of Al element. Results showed that the proportion of Al in PCN-AA5, PCN-AA10, PCN-AA20 and PCN-AA30 was 0.16 %, 0.27 %, 0.39 % and 0.52 %, respectively. This indicated that with the increased amount of $Al(aa)_3$ added during the material preparation process, Al element was successfully doped into the PCN structure, which could provide new metal coordination sites for the reaction system. The microstructure of PCN-AA was observed by SEM and TEM (Fig. 2). Taking PCN-AA0 and PCN-AA30 as examples, the photocatalytic materials exhibited a typical sheet-like stacked curl structure of carbon nitride. Due to the small addition of aluminium acetylacetonate, there was no significant difference in the microstructure of these two materials. However, compared with PCN-AA0, PCN-AA30 had some obvious pores, which may provide more active sites for the photocatalytic reaction. It can also be seen from the element mapping results of PCN-AA30 that Al has been effectively

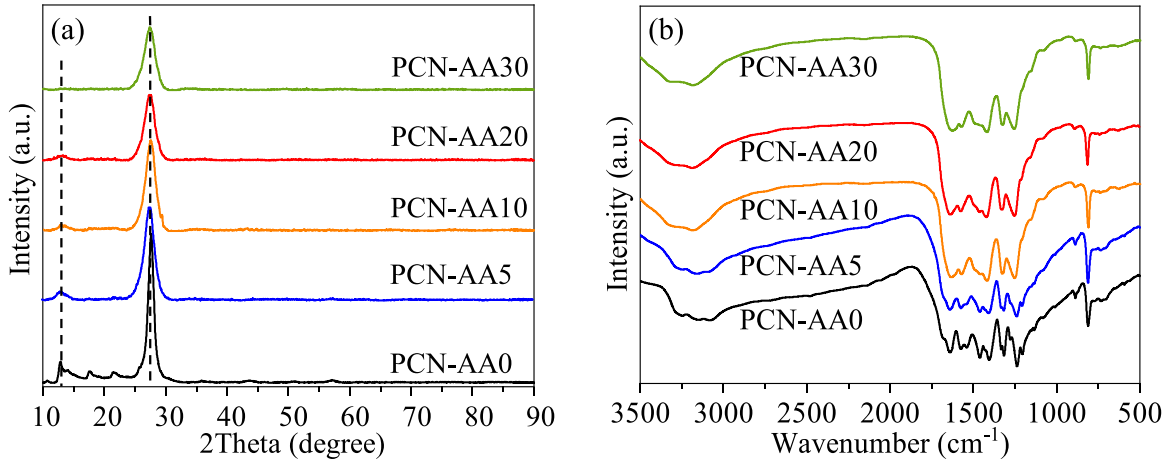

Fig. 1. XRD patterns (a) and FT-IR spectra (b) of PCN-AA materials.

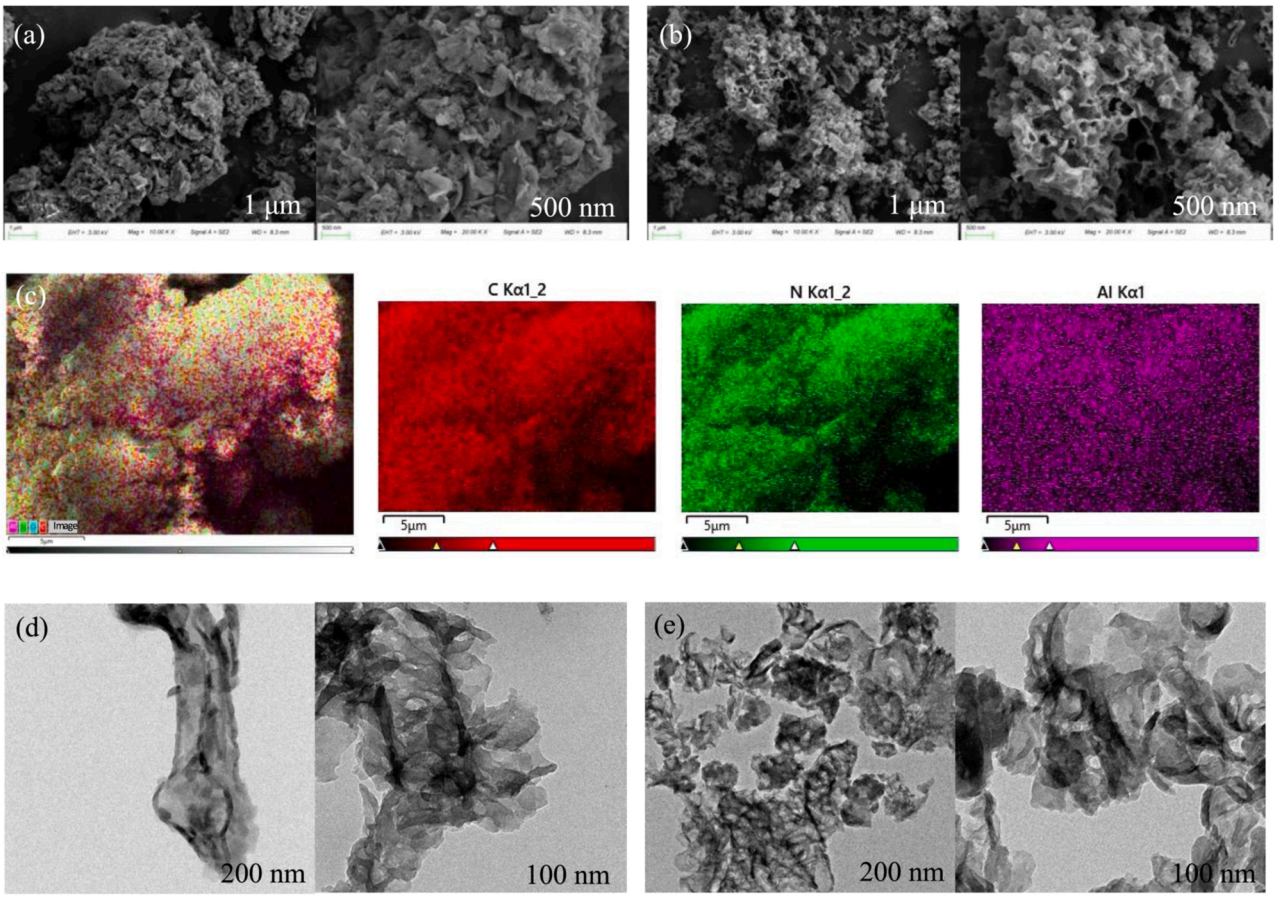

Fig. 2. SEM images of PCN-AA0 (a) and PCN-AA30 (b), the element mapping images of PCN-AA30 (c), TEM images of PCN-AA0 (d) and PCN-AA30 (e).

dispersed on the material sample. In addition, parameters such as the specific surface area, total pore volume and adsorption average pore diameter of PCN-AA were measured by BET-nitrogen adsorption method in this study, and the isotherm adsorption-desorption curves can be seen in Fig. S2. The results (Table S4) showed that the BET surface area of PCN-AA10 and PCN-AA20 was smaller than the original PCN, but the total pore volume and average pore diameter were increased. When the addition of $Al(aa)_3$ increased to a certain extent, the BET parameters of the material become significantly larger. The specific surface area and total pore volume of PCN-AA30 were 108.66 $m^2\ g^{-1}$ and 0.3023 $cm^3\ g^{-1}$, respectively, which were larger than 61.74 $m^2\ g^{-1}$ and 0.1597 $cm^3\ g^{-1}$ of PCN-AA0. Combined with the SEM images, the increase of specific surface area and pore volume of PCN-AA30 could highly improve the efficiency of photocatalysis.

This study also used XPS to analyse the surface chemical composition and state of PCN-AA photocatalytic materials. The XPS survey spectrum of PCN-AA0, PCN-AA10 and PCN-AA30 are shown in Fig. S3, and the high-resolution XPS spectra of C 1s, O 1s, N1s and Al 2p are shown in Fig. 3. PCN-AA0 was only composed of C, N and O elements, while PCN-AA10 and PCN-AA30 contained characteristic peaks of C, N, O and Al elements, which also indicated that Al has been successfully doped in the PCN structure. In the C 1s spectrum, the peaks at 288.1 eV, 286.6 eV and 284.6 eV of PCN-AA10 and PCN-AA30 were corresponded to sp^2 hybridized carbon (N-C═N), C-O or C-OH of hydroxylated carbon and alkyl carbons (C═C-C or C-H), respectively [34, 40–42]. The peak intensity at the binding energy of 286.6 eV has increased, which should be caused by the hydroxylated carbon in the structure formed by in situ keto-enol cyclization of urea and acetylacetone. There was only one main peak for the three material samples in the O 1s spectrum, and the peak moved from 531.9 eV of PCN-AA0 to 531.7 eV of PCN-AA30, which was attributed to N-C-O [35], and the peak intensity increased with the doping of $Al(aa)_3$. In the N 1s spectrum, the binding energies of the samples all changed slightly. The peaks at 401.0 eV, 400.0 eV and 398.6 eV in PCN-AA30 material were corresponded to the amino group ($C\text{-}NH_2$), tertiary nitrogen ($N\text{-}C_3$) and sp^2 hybridized nitrogen (C═N-C) [43]. In addition, although the doping amount of $Al(aa)_3$ was relatively small, the tiny peaks could still be observed in the Al 2p spectra of PCN-AA10 and PCN-AA30.

3.1.2. *Optical absorption properties*

The optical absorption properties of photocatalytic materials were analysed by UV-Vis. Taking PCN-AA0, PCN-AA10, PCN-AA20 and PAN-A30 as examples (Fig. 4(a)), with increasing $Al(aa)_3$ doping amount, the response value of the materials in visible light region has been significantly improved, and the wavelength of light absorption has also undergone a significant red shift. It showed that the introduction of aluminium acetylacetonate effectively improved the light absorption efficiency of the PCN, and making it exhibit the enhanced absorption in visible light range, which was similar to the results described in the literature [44,45]. In addition, combined with the analysis of Fig. 4(b), the colour of the samples deepens continuously from the creamy yellow of PCN-AA0 to the dark yellow of PCN-AA30, which was also consistent with the results of UV-Vis.

It could be seen from the PL spectra in Fig. 4(c) that the PL intensity of PCN-AA was significantly lower than the original PCN-AA0, and the intensity of characteristic peaks gradually decreased with the increase of $Al(aa)_3$ doping amount. This indicated that after the composite of aluminium acetylacetonate, the photo-generated electron and hole recombination rate of the material was reduced, then the photocatalytic property was improved. At the same time, the characteristic peak of the material was red shifted from 462 nm of PCN-AA0 to 508 nm of PCN-AA30, which was mainly due to the expansion of the π-conjugated

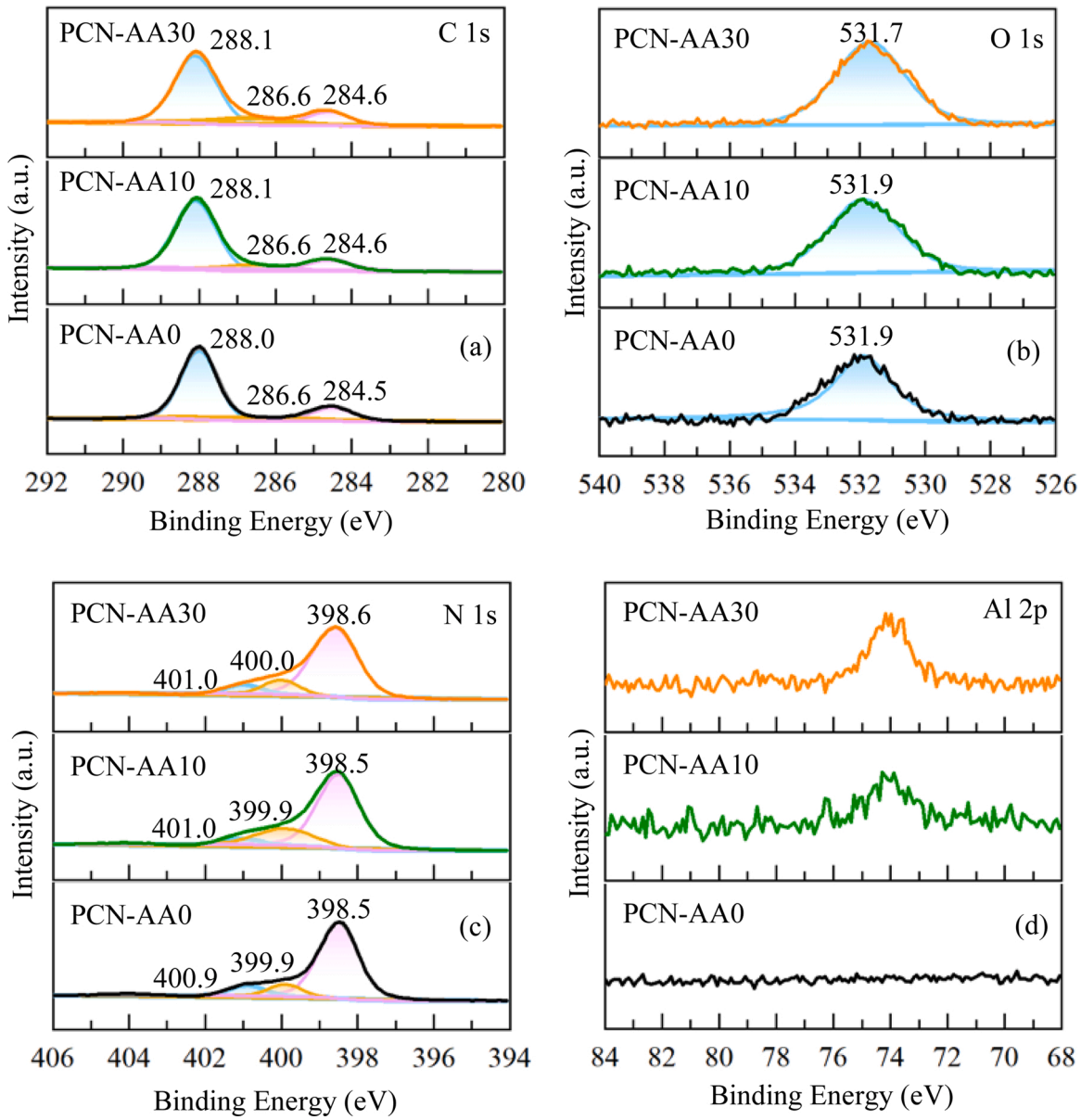

Fig. 3. High-resolution XPS spectra of C 1s (a), O 1s (b), N 1s (c) and Al 2p (d) for PCN-AA0, PCN-AA10 and PCN-AA30.

system [46].

3.2. Photocatalytic degradation and kinetics of different material ratios

It can be seen from the characterization results that there were certain differences in the microstructure and chemical properties of the PCN-AA materials with different ratios. In order to study the effect of material ratio on the photocatalytic effect, the TCS degradation efficiency of PCN-AA was compared under the simulated visible light irradiation conditions. The variation curves of TCS residual ratio (C/C_0) with the reaction time are shown in Fig. 5(a). With the increase doping amount of $Al(aa)_3$, the photocatalytic degradation kept increasing, and the TCS percentage removals of five materials were all greater than 90 % after 120 min. And under the action of PCN-AA30, only 0.71 % of TCS remained at 90 min. In addition, although the detection results of TCS had some fluctuations in the blank control group without adding any material, it could still be considered that there was almost no visible light degradation of TCS under the experimental conditions.

By fitting the reaction kinetics of the photocatalytic degradation of PCN-AA, it can be found that the reaction conformed to the pseudo-first-order kinetic characteristics (Fig. 5(b)), and the reaction rate constant k value is shown in Table 1. The fastest reaction rate was PCN-AA30 ($k = 0.0529\ min^{-1}$), which was 2.45 times that of PCN-AA0 ($k = 0.0216\ min^{-1}$), indicating that the interaction between PCN and $Al(aa)_3$ could effectively improve the photocatalytic performance of the materials under visible light, which was also consistent with the results of characterization. Therefore, PCN-AA30 was selected as the optimal material for degrading TCS in the subsequent experiments.

3.3. Effects of different factors on photocatalytic degradation of TCS

In order to study the effects of different reaction parameters in the photocatalytic degradation of TCS, five influencing factors including catalyst dosage, initial TCS concentration, pH, common inorganic anions and natural organic matter (NOM) in water were investigated. The variation curves of TCS residual ratio (C/C_0) with the reaction time under each factor are shown in Fig. 6(a–e), and the degradation kinetic curves (Fig. S4) and their reaction rate constant k values (Table S5) are shown in the Supplementary Material.

When the concentration of PCN-AA30 in the reaction system ranged

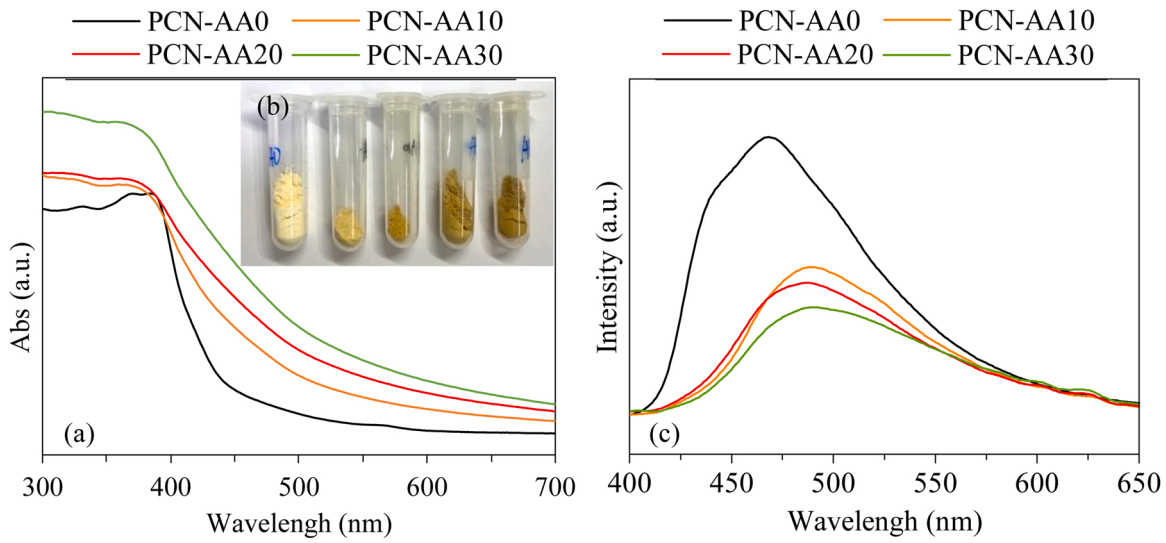

Fig. 4. UV–vis spectra of PCN-AA (a), photograph of PCN-AA (b) (from left to right were PCN-AA0, PCN-AA5, PCN-AA10, PCV-AA20 and PCN-AA30); PL spectra of PCN-AA (c).

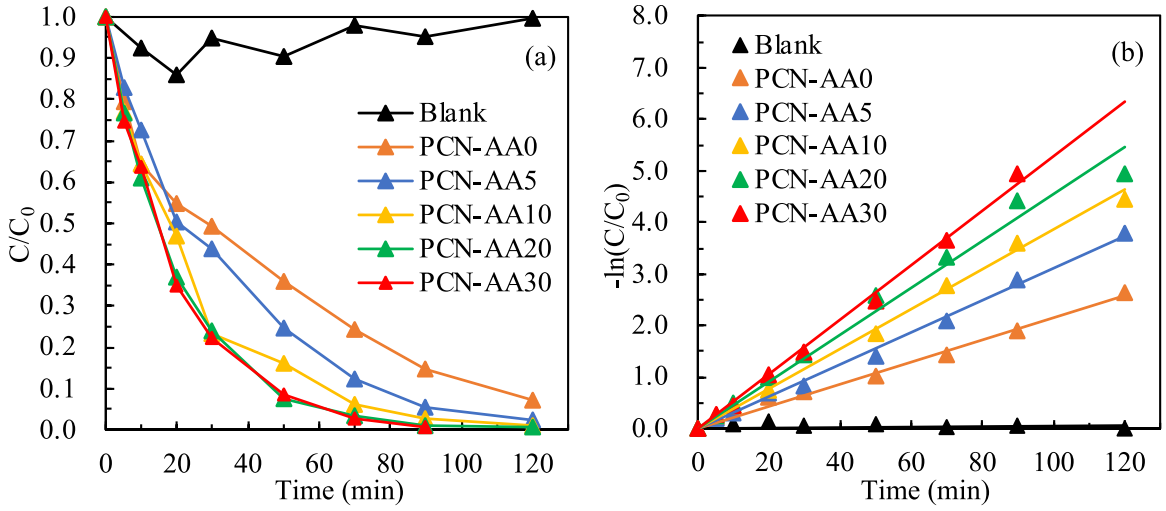

Fig. 5. Photocatalytic effects (a) and kinetics (b) of different material ratios (All the beginning of time was after reaching the adsorption-desorption equilibrium under dark conditions for 30 min).

Table 1
Photocatalytic degradation reaction rate constant k of different material ratios.

Materials	PCN-AA0	PCN-A5	PCN-AA10	PCN-AA20	PCN-AA30
k (min^{-1})	0.0216	0.0311	0.0386	0.0454	0.0529

from 100 mg L^{-1} to 400 mg L^{-1}, the degradation effects of TCS were significantly improved (Fig. 6(a)), and the reaction rate constant increased from 0.0382 min^{-1} to 0.0631 min^{-1}, indicating that the catalyst dosage was proportional to the reactive sites in the system. However, when the material concentration reached a certain amount (300 mg L^{-1}), the growth of photocatalytic reaction rate was obviously slowed down, which due to the light transmittance of the solution might be affected when the dosage was too large, so that the reaction rate could not continue to increase significantly [47].

As the initial concentration of TCS increased from 1 mg L^{-1} to 5 mg L^{-1} (Fig. 6(b)), the photocatalytic degradation efficiency dropped and the reaction rate constant decreased from 0.0912 min^{-1} to 0.0233 min^{-1}. In this case, a certain amount of photocatalytic active sites in the reaction system were easily occupied by higher concentration of pollutants, resulting in the blocking of the photocatalytic reaction [48]. At the same time, in the process of degrading higher concentration of TCS, more intermediate products may be produced and these substances will also compete with TCS for the active species, causing a decrease in the degradation rate.

The effect of pH on the TCS degradation of is shown in Fig. 6(c). In the experimental group with pH = 6, dilute hydrochloric acid or NaOH was not added for adjustment, and it could be used as the control group. When the reaction system was acidic (pH = 4), the degradation rate of photocatalysis increased, while the alkaline conditions (pH = 8 and pH = 10) reduced the reaction rate, and the alkalinity of solution was inversely proportional to the degradation efficiency. This was mainly due to the fact that TCS will be converted into TCS anion under alkaline conditions, and the surface of materials was negatively charged at this time, so the electrostatic repulsion between them may reduce their mutual contact, thus affecting the effect of photocatalytic degradation [49]. However, un-dissociated species of TCS was ubiquitous and easily oxidized in the case of lower pH, which was more conducive to the photocatalytic degradation [50].

The effects of common inorganic anions in water were simulated by

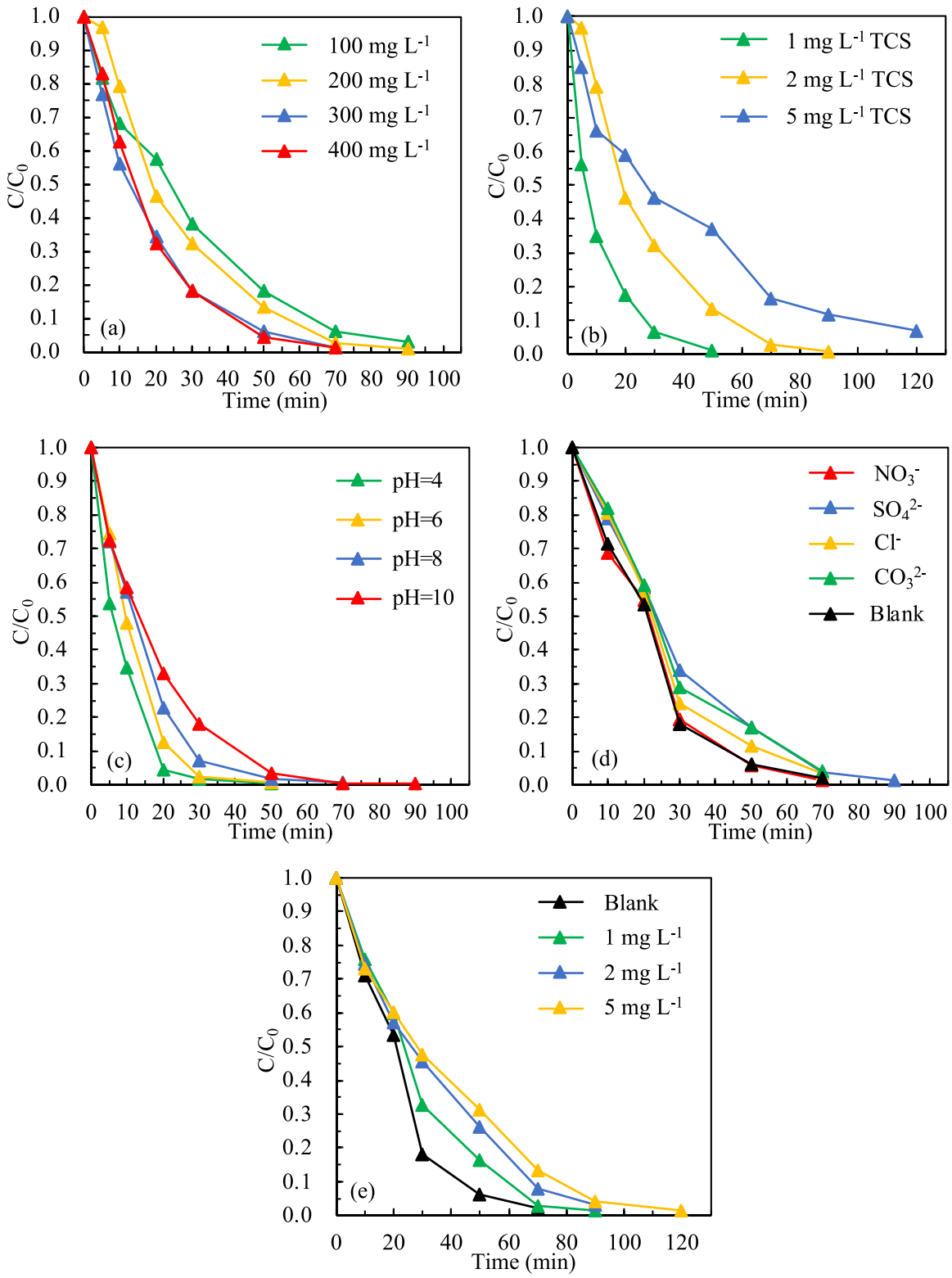

Fig. 6. Effects of catalyst dosage (a), initial concentration of TCS (b), pH (c), common inorganic anions (d) and NOM simulated by humic acid (e) on photocatalytic degradation (All the beginning of time was after reaching the adsorption-desorption equilibrium under dark conditions for 30 min).

adding $NaNO_3$, Na_2SO_4, Na_2CO_3 and NaCl to the reaction system, and the initial concentration of each anion was 5 mmol L^{-1}. SO_4^{2-}, Cl^- and CO_3^{2-} had certain inhibitory effects on the photocatalytic reaction, and the inhibition rates were 19.3 %, 16.7 % and 25.0 %, respectively (Fig. 6 (d)). Only NO_3^- slightly promoted the photodegradation of TCS, and k value changed from 0.0545 min^{-1} in the blank control to 0.0576 min^{-1}. This may be attributed to the fact that NO_3^- was an efficient electron acceptor, which inhibited the recombination of photogenerated electrons and holes in the reaction system, thereby increasing the reaction rate. SO_4^{2-} may be easily adsorbed on the surface of materials and cause their inactivation, thereby inhibiting the photocatalytic reaction. The presence of Cl^- may compete with pollutants for active species (such as

h^+), resulting in the photocatalytic reaction rate to decrease [51]. The inhibitory effect of CO_3^{2-} may be due to its hydrolysis leading to an increase in pH of the solution. However, alkaline conditions were not conducive to the degradation of TCS [51].

The effect of NOM in water was simulated by humic acid on the photocatalytic degradation, and the concentration of humic acid in each experimental group was 1 mg L^{-1}, 2 mg L^{-1} and 5 mg L^{-1}, respectively. With the increase of humic acid concentration, the degradation rate of TCS decreased continuously, and the inhibition rate of photocatalytic reaction reached a maximum of 40.4 % (Fig. 6(e)). The presence of NOM in the reaction system may compete with pollutants for photons, and had a certain quenching effect on active species, thus inhibiting the photocatalytic degradation [52]. It can be inferred that if the photocatalytic technologies are implemented to remove multiple pollutants in the actual water body, the degradation effect on specific pollutants may be affected.

3.4. The photocatalytic degradation mechanism of TCS by PCN-AA

The radicals quencher experiments were carried out to identify the active species that played a major role in the degradation of TCS by PCN-AA30 photocatalytic material. The principle of applying quenchers is that they can specifically bind to the radicals and generate stable or persistent intermediates, acting as scavengers to inhibit the reactions between active species and target pollutants significantly [53]. Based on published studies, 1,4-benzoquinone was chosen as the quencher for $\cdot O_2^-$, isopropanol (IPA) was the quencher for ·OH and ethylenediaminetetraacetic acid disodium (EDTA-2Na) was the quencher for photogenerated holes h^+ [19]. The concentrations of these three quenchers in the reaction system were 5 mmol L^{-1}. The residual ratios (C/C_0) of TCS at the end of the photocatalytic reaction are shown in Fig. 7(a). The degradation rate of TCS was only 8.00 % in the experimental group containing 1,4-Benzoquinone, and the photocatalytic activity of PCN-AA30 was almost completely inhibited, indicating that the main oxidative ability of this photocatalyst was closely related to the effect of superoxide radicals in the reaction system. This is probably because the Al element doped in PCN transferred the conduction band (CB) electron to O_2, thereby generating more superoxide radicals [54]. h^+ played a secondary role in the reaction system, and 50.14 % of TCS remained under the action of EDTA-2Na. However, the addition of IPA hardly affects the photocatalytic degradation process of TCS, indicating that ·OH has little effect.

Furthermore, in order to confirm the existence of active species, electron paramagnetic resonance (EPR) was used to measure free radicals in the photocatalytic reaction system. Using 5,5-dimethyl-1-pyrroline-N-oxide (DMPO) as a spin trap to measure the EPR signals of DMPO- $\cdot O_2^-$ and DMPO- ·OH, and the generation of h^+ was detected using 2,2,6,6-tetramethylpiperidinyloxy (TEMPO) as a marker. Fig. 7 (b–d) shows the EPR spectra of PCN-AA30 material under the visible light. The EPR signals of $\cdot O_2^-$ and ·OH could not be observed under the dark condition, indicating that these two active species were not generated during the dark reaction. But under the light condition, the characteristic signals of DMPO- $\cdot O_2^-$ adduct and DMPO- ·OH adduct appeared obviously at 5 min and 10 min, and the signal of $\cdot O_2^-$ was slightly irregular but relatively stable. Although the results of radicals quencher experiment showed that ·OH had no effect on the photocatalytic degradation of TCS, this did not affect its existence in the reaction system. For h^+, since TEMPO was an oxide of 2,2,6,6-Tetramethylpiperidine (TEMP), and a significant signal of h^+ can be detected under dark conditions. When the light was turned on, h^+ generated by the reaction system would react with TEMPO, and the detection results showed that the signal would be gradually weakened with the prolongation of illumination time. This also indicated that the photogenerated holes were persistent, which contributed to the improvement of photocatalytic activity [55].

Combined with the above analysis and related literature [53,54], the

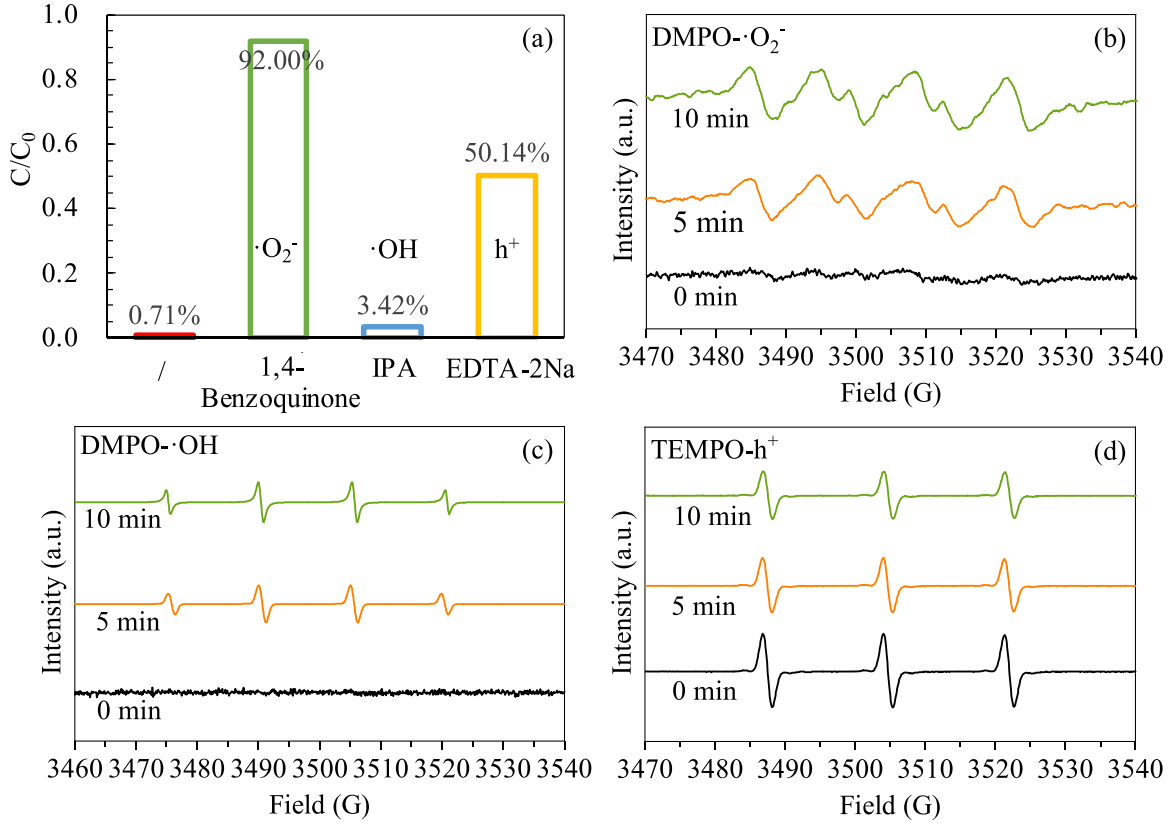

Fig. 7. Radicals quencher experiment results (a); EPR spectra of DMPO- $\cdot O_2^-$ adduct (b), DMPO- ·OH adduct (c) and TEMPO-h^+ adduct (d).

basic mechanism of TCS degradation by PCN-AA photocatalytic materials in the reaction system is shown in formulas (2)-(6). Under the irradiation of visible light, the material absorbed visible light to generate the photogenerated electron-hole pairs, and they were rapidly separated. Photogenerated electrons can react with O_2 in the reaction system to form $\cdot O_2^-$, and some $\cdot O_2^-$ can further react with H^+ and e^- to form H_2O_2 and ·OH. Subsequently, the generated $\cdot O_2^-$, h^+ and ·OH resulted in the degradation of TCS.

$$PCN\text{-}AA30 + h\nu \rightarrow e^- + h^+ \quad (2)$$

$$e^- + O_2 \rightarrow \cdot O_2^- \quad (3)$$

$$\cdot O_2^- + 2H^+ + e^- \rightarrow H_2O_2 \quad (4)$$

$$H_2O_2 + e^- \rightarrow \cdot OH + OH^- \quad (5)$$

$$TCS + \cdot O_2^- / h^+ / \cdot OH \rightarrow \text{degradation products} \quad (6)$$

Table 2
Degradation products from the photocatalytic degradation of TCS.

No.	Abbreviation	m/z [M-H]$^-$	Retention time	Formula	Proposed structure
1	TCS	286.94	14.15 min	$C_{12}H_7Cl_3O_2$	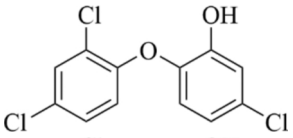
2	DP316	316.92	15.30 min	$C_{12}H_5Cl_3O_4$	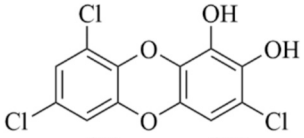
3	DP251	251.01	15.30 min	$C_{12}H_9ClO_4$	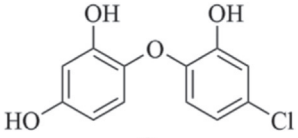
4	DP250	250.96	15.30 min	$C_{12}H_6Cl_2O_2$	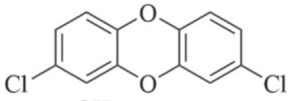
5	DP160	160.96	7.65 min	$C_6H_4Cl_2O$	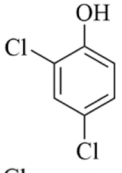
6	DP144	144.96	7.65 min	$C_6H_4Cl_2$	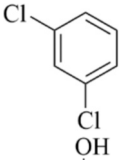
7	DP142–1	142.99	7.65 min	$C_6H_5ClO_2$	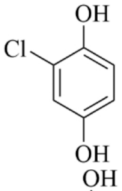
8	DP142–2	142.99	7.65 min	$C_6H_5ClO_2$	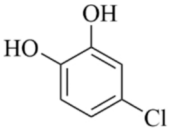
9	DP126	126.99	14.15 min	C_6H_5ClO	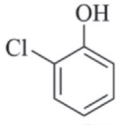
10	DP109	109.03	7.65 min	$C_6H_6O_2$	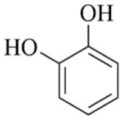
11	DP93	93.03	7.65 min	C_6H_6O	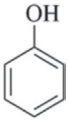

3.5. The degradation pathway of TCS and its degradation products

The degradation products formed during the photocatalytic degradation of TCS by PCN-AA30 were investigated by UPLC-Q-TOF. Combined with the HPLC detection results, the samples corresponding to the six time points of the TCS residual percentages, about 100 %, 70 %, 50 %, 30 %, 10 % and 0 %, in the reaction process were selected for analysis (the example mass spectra are shown in Fig. S5). According to the results of Q-TOF data and related studies [32,56–58], the mass-to-charge ratio, retention time and structure analysis of possible degradation intermediates in the process of photocatalytic degradation are shown in Table 2, and the inferred TCS degradation pathway is shown in Fig. 8. Moreover, the main pathways for the photocatalytic degradation of TCS are described as follows.

The active species (such as $\cdot O_2^-$) caused the splitting of the carbon-oxygen bond to form DP160 (2,4-dichlorophenol), and then generating DP142–2 (4-chlorocatechol) [59], DP142–2 may further dechlorination generated DP109. DP160 had two degradation methods, one was to form DP126 (chlorophenol) through dechlorination reaction, the continuous dechlorination reactions of DP126 may form DP93 (phenol); and the other one was to generate DP144 (1,3-dichlorbenzene) by free radicals attack and cleavage of aromatic ring [60].

3.6. The safety assessment of PCN-AA

The original purpose of studying photocatalytic technology to degrade micro-pollutants in water was to reduce the potential ecological risks and possible health risks to the human body, and exploring the application feasibility of photocatalysis at the same time. In this process, the safety of the photocatalytic material itself was also worth investigating. Therefore, the luminescent bacteria method was used to test the acute biological toxicity of PCN-AA materials with different concentrations in this study.

According to the acute toxicity grade, the highest luminescent inhibition ratio was 29.56 % when the concentration of PCN-AA30 material reached 300 mg L^{-1}, and all the test results were in the low toxicity range. Considering that the PCN-AA materials themselves were yellow to varying degrees, their mixed suspensions will also appear yellow. With the increase of the material concentrations, the light transmittance of suspensions gradually decreased, so it would have a certain influence on the experimental results. Therefore, according to the luminescent inhibition ratio in Table 3, it could be inferred that the acute biological toxicity of the photocatalytic materials in the reaction system was low, and their safety was relatively high if the practical engineering application would be considered in the future.

4. Conclusions

In this work, aluminium acetylacetonate was doped into the PCN structure by a facile method. The photocatalytic performance of the material could be efficiently improved under visible light, and the reactive sites also be increased. Therefore, a higher degradation efficiency for TCS could be achieved. PCN-AA materials with different ratios could degrade more than 90 % of TCS at 120 min, especially the removal rate of PCN-AA30 was 99.29 %. The degradation of TCS under visible light was promoted when the catalyst dosage was increased, pH was decreased or NO_3^- was present. And the inhibitory effect would occur when the concentration of TCS or pH was increased, SO_4^{2-}, Cl^-, CO_3^{2-} or NOM was present. This indicated that the removal effect of micro-pollutants in water would be affected by various factors in the photocatalytic reaction system. The mechanism analysis of photocatalysis showed that $\cdot O_2^-$ was the main active radical in the photocatalytic process, while h^+ and ·OH played the secondary role in the reaction system. In addition, the possible 10 degradation products of TCS and their degradation pathways were determined by UPLC-Q-TOF. The PCN-AA

Table 3
Luminescent inhibition ratio of photocatalytic materials (%).

Catalyst dosage	PCN-AA0	PCN-AA5	PCN-AA10	PCN-AA20	PCN-AA30
300 mg L^{-1}	21.65	22.59	27.13	16.34	29.56
200 mg L^{-1}	8.08	7.69	12.06	4.10	18.34
100 mg L^{-1}	-2.34	1.30	3.72	1.94	5.34

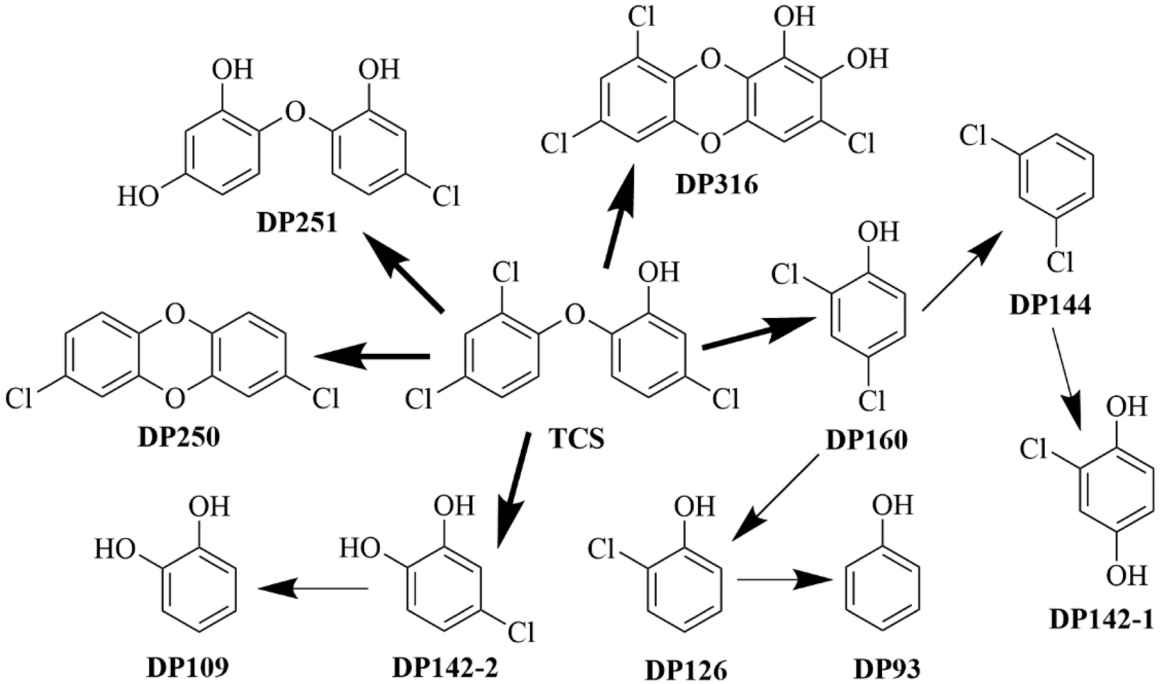

Fig. 8. Possible pathways for the photocatalytic degradation of TCS.

materials could not only effectively degrade TCS, but also had relatively high safety to biology, which may provide a feasible approach and reference for the practical application of photocatalytic removal of micro-pollutants in the future.

CRediT authorship contribution statement

Danyan Sun: Conceptualization, Methodology, Validation, Formal analysis, Investigation, Data curation, Writing – original draft, Writing – review & editing, Visualization. **Xiaohu Lin:** Conceptualization, Methodology, Resources, Writing – review & editing, Supervision. **Jingcheng Xu:** Methodology, Supervision, Project administration, Funding acquisition. **Zhibo Lu:** Resources, Supervision. **Juwen Huang:** Supervision, Project administration. **Shiyi Li:** Resources, Supervision. **Luiza C. Campos:** Supervision, Writing – original draft, Writing – review & editing.

Declaration of Competing Interest

The authors declare that they have no known competing financial interests or personal relationships that could have appeared to influence the work reported in this paper.

Data Availability

Data will be made available on request.

Acknowledgements

This research was supported by the scholarship from the China Scholarship Council (CSC) (Grant No. 202106260198) and PowerChina Huadong Engineering Corporation Limited (KY2018-SHJ-02).

Appendix A. Supporting information

Supplementary data associated with this article can be found in the online version at doi:10.1016/j.jece.2022.109186.

References

[1] C. Stamm, K. Räsänen, F.J. Burdon, F. Altermatt, J. Jokela, A. Joss, M. Ackermann, R.I.L. Eggen, Unravelling the impacts of micropollutants in aquatic ecosystems: interdisciplinary studies at the interface of large-scale ecology, Adv. Ecol. Res. 55 (2016) 183–223, https://doi.org/10.1016/bs.aecr.2016.07.002.

[2] Y. Liu, M. Ji, R. Wang, H. Zhai, S. Yu, B. Liu, Y. Zhao, Spatial distribution and comprehensive evaluation of emerging organic pollutants in effluents from wastewater treatment plants in northern cities of China, Desalin. Water Treat. 156 (2019) 20–31, https://doi.org/10.5004/dwt.2019.24095.

[3] A. Bianco, D. Fabbri, M. Minella, M. Brigante, G. Mailhot, V. Maurino, C. Minero, D. Vione, New insights into the environmental photochemistry of 5-chloro-2-(2,4-dichlorophenoxy)phenol (triclosan): reconsidering the importance of indirect photoreactions, Water Res. 72 (2015) 271–280, https://doi.org/10.1016/j.watres.2014.07.036.

[4] P. Gautam, J.S. Carsella, C.A. Kinney, Presence and transport of the antimicrobials triclocarban and triclosan in a wastewater-dominated stream and freshwater environment, Water Res. 48 (2014) 247–256, https://doi.org/10.1016/j.watres.2013.09.032.

[5] Y. Gao, Y. Ji, G. Li, T. An, Mechanism, kinetics and toxicity assessment of OH-initiated transformation of triclosan in aquatic environments, Water Res. 49 (2014) 360–370, https://doi.org/10.1016/j.watres.2013.10.027.

[6] Y. Yang, W. Liu, Y. Liu, J. Zhao, Q. Zhang, M. Zhang, J. Zhang, Y. Jiang, L. Zhang, G. Ying, Suitability of pharmaceuticals and personal care products (PPCPs) and artificial sweeteners (ASs) as wastewater indicators in the Pearl River Delta, South China, Sci. Total Environ. 590 (2017) 611–619, https://doi.org/10.1016/j.scitotenv.2017.03.001.

[7] P.A. Fair, H.B. Lee, J. Adams, C. Darling, G. Pacepavicius, M. Alaee, G.D. Bossart, N. Henry, D. Muir, Occurrence of triclosan in plasma of wild Atlantic bottlenose dolphins (Tursiops truncatus) and in their environment, Environ. Pollut. 157 (2009) 2248–2254, https://doi.org/10.1016/j.envpol.2009.04.002.

[8] X. Lin, J. Xu, A.A. Keller, H. Li, Y. Gu, W. Zheng, D. Sun, Z. Lu, J. Wang, X. Huang, G. Li, Occurrence and risk assessment of emerging contaminants in a water reclamation and ecological reuse project, Sci. Total Environ. 744 (2021), 140977, https://doi.org/10.1016/j.scitotenv.2020.140977.

[9] L.M. Weatherly, J.A. Gosse, Triclosan exposure, transformation, and human health effects, J. Toxicol. Environ. Health 20 (2017) 447–469, https://doi.org/10.1080/10937404.2017.1399306.

[10] P. Iovino, S. Chianese, M. Prisciandaro, D. Musmarra, Triclosan photolysis: operating condition study and photo-oxidation pathway, Chem. Eng. J. 377 (2019), 121045, https://doi.org/10.1016/j.cej.2019.02.132.

[11] Z. Luo, Y. He, D. Zhi, L. Luo, Y. Sun, E. Khan, L. Wang, Y. Peng, Y. Zhou, D.C. W. Tsang, Current progress in treatment techniques of triclosan from wastewater: a review, Sci. Total Environ. 696 (2019), 133990, https://doi.org/10.1016/j.scitotenv.2019.133990.

[12] N.O. Dos Santos, L.A.C. Teixeira, J.C. Spadotto, L.C. Campos, A simple ZVI-Fenton pre-oxidation using steel-nails for NOM degradation in water treatment, J. Water Process Eng. 43 (2021), 102230, https://doi.org/10.1016/j.jwpe.2021.102230.

[13] T. Methatham, M. Lu, C. Ratanatamskul, Effect of operating parameters on triclosan degradation by Fenton's reagents combined with an electrochemical system, Desalin. Water Treat. 52 (2014) 920–928, https://doi.org/10.1080/19443994.2013.827308.

[14] A. Butkovskyi, A.W. Jeremiasse, L.H. Leal, T.V.D. Zande, H. Rijnaarts, G. Zeeman, Electrochemical conversion of micropollutants in gray water, Environ. Sci. Technol. 48 (2014) 1893–1901, https://doi.org/10.1021/es404411p.

[15] X. Xie, C. Chen, X. Wang, J. Li, S. Naraginti, Efficient detoxification of triclosan by a S-Ag/TiO_2@g-C_3N_4 hybrid photocatalyst: process optimization and bio-toxicity assessment, RSC Adv. 35 (2019) 20439–20449, https://doi.org/10.1039/C9RA03279G.

[16] A.G. Capodaglio, Critical perspective on advanced treatment processes for water and wastewater: AOPs, ARPs, and AORPs, Appl. Sci. 10 (2020) 4549, https://doi.org/10.3390/app10134549.

[17] R. Bariki, D. Majhi, K. Das, A. Beherab, B.G. Mishra, Facile synthesis and photocatalytic efficacy of UiO-66/$CdIn_2S_4$ nanocomposites with flowerlike 3D-microspheres towards aqueous phase decontamination of triclosan and H_2 evolution, Appl. Catal. B Environ. 270 (2020), 118882, https://doi.org/10.1016/j.apcatb.2020.118882.

[18] O. Legrini, E. Oliveros, A.M. Braun, Photochemical processes for water-treatment, Chem. Rev. 93 (1993) 671–698, https://doi.org/10.1021/cr00018a003.

[19] A.A. Isari, M. Mehregan, S. Mehregan, F. Hayati, R.R. Kalantary, B. Kakavandi, Sono-photocatalytic degradation of tetracycline and pharmaceutical wastewater using WO_3/CNT heterojunction nanocomposite under US and visible light irradiations: a novel hybrid system, J. Hazard. Mater. 390 (2020), 122050, https://doi.org/10.1016/j.jhazmat.2020.122050.

[20] X. Wei, X. Xu, X. Yang, Z. Liu, S. Naraginti, S. Lin, W. Song, B. Li, Novel assembly of $BiVO_4$@N-Biochar nanocomposite for efficient detoxification of triclosan, Chemosphere 298 (2022), 134292, https://doi.org/10.1016/j.chemosphere.2022.134292.

[21] H. Fu, K.A. Gray, TiO_2 (core)/crumpled graphene oxide (shell) nanocomposites show enhanced photodegradation of carbamazepine, Nanomaterials 11 (2021) 2087, https://doi.org/10.3390/nano11082087.

[22] S. Dong, G.J. Lee, R. Zhou, J.J. Wu, Synthesis of g-C_3N_4/$BiVO_4$ heterojunction composites for photocatalytic degradation of nonylphenol ethoxylate, Sep. Purif. Technol. 250 (2020), 117202, https://doi.org/10.1016/j.seppur.2020.117202.

[23] Á. Tolosana-Moranchel, A. Manassero, M.L. Satuf, O. M.Alfano, J. A.Casas, A. Bahamonde, Influence of TIO_2-rGO optical properties on the photocatalytic activity and efficiency to photodegrade an emerging pollutant, Appl. Catal. B Environ. 246 (2019) 1–11, https://doi.org/10.1016/j.apcatb.2019.01.054.

[24] I. Köwitsch, M. Mehring, Carbon nitride materials: impact of synthetic method on photocatalysis and immobilization for photocatalytic pollutant degradation, J. Mater. Sci. 56 (2021) 18608–18624, https://doi.org/10.1007/s10853-021-06405-z.

[25] C. Zhou, G. Zeng, D. Huang, Y. Luo, M. Cheng, Y. Liu, W. Xiong, Y. Yang, B. Song, W. Wang, B. Shao, Z. Li, Distorted polymeric carbon nitride via carriers transfer bridges with superior photocatalytic activity for organic pollutants oxidation and hydrogen production under visible light, J. Hazard. Mater. 386 (2019), 121947, https://doi.org/10.1016/j.jhazmat.2019.121947.

[26] C. Xu, W. Zhang, K. Deguchi, S. Ohki, T. Shimizu, R. Ma, T. Sasaki, Construction of a push–pull system in g-C_3N_4 for efficient photocatalytic hydrogen evolution under visible light, J. Mater. Chem. A 8 (2020) 13299–13310, https://doi.org/10.1039/C9TA13513H.

[27] K. Li, Y. Jiang, W. Rao, Y. Li, X. Liu, J. Zhang, X. Xu, K. Lin, Cooperative coupling strategy for constructing 0D/2D carbon nitride composites with strengthened chemical interaction for enhanced photocatalytic applications, Chem. Eng. J. 431 (2022), 134075, https://doi.org/10.1016/j.cej.2021.134075.

[28] W. Zhen, X. Yuan, X. Ning, X. Gong, C. Xue, Building oxime-Ni^{2+} complex on polymeric carbon nitride: molecular-level design of highly efficient hydrogen generation photocatalysts, ACS Appl. Mater. Interfaces 12 (2020) 868–876, https://doi.org/10.1021/acsami.9b18856.

[29] J. Cheng, Z. Hu, Q. Li, X. Li, S. Fang, X. Wu, M. Li, Y. Ding, B. Liu, C. Yang, L. Wen, Y. Liu, K. Lv, Fabrication of high photoreactive carbon nitride nanosheets by polymerization of amidinourea for hydrogen production, Appl. Catal. B Environ. 245 (2019) 197–206, https://doi.org/10.1016/j.apcatb.2018.12.044.

[30] O. Fontelles-Carceller, M.J. Muñoz-Batista, M. Fernández-García, A. Kubacka, Interface effects in sunlight-driven Ag/g-C_3N_4 composite catalysts: study of the toluene photodegradation quantum efficiency, ACS Appl. Mater. Interfaces 8 (4) (2016) 2617–2627, https://doi.org/10.1021/acsami.5b10434.

[31] K.V. Savunthari, D. Arunagiri, S. Shanmugam, S. Ganesan, M.V. Arasu, N.A. Al-Dhabi, N.T.L. Chi, V.K. Ponnusamy, Green synthesis of lignin nanorods/g-C_3N_4 nanocomposite materials for efficient photocatalytic degradation of triclosan in

environmental water, Chemosphere 272 (2021), 129801, https://doi.org/10.1016/j.chemosphere.2021.129801.
[32] A. Yuval, F. Eran, W. Janin, O. Oliver, D. Yael, Photodegradation of micropollutants using V-UV/UV-C processes; triclosan as a model compound, Sci. Total Environ. 601–602 (2017) 397–404, https://doi.org/10.1016/j.scitotenv.2017.05.172.
[33] J.C. Yu, T.Y. Kwong, Q. Luo, Z. Cai, Photocatalytic oxidation of triclosan, Chemosphere 65 (2006) 390–399, https://doi.org/10.1016/j.chemosphere.2006.02.011.
[34] Y. Yang, C. Zhang, D. Huang, G. Zeng, J. Huang, C. Lai, C. Zhou, W. Wang, H. Guo, W. Xue, R. Deng, M. Cheng, W. Xiong, Boron nitride quantum dots decorated ultrathin porous g-C_3N_4: intensified exciton dissociation and charge transfer for promoting visible-light-driven molecular oxygen activation, Appl. Catal. B Environ. 245 (2019) 87–99, https://doi.org/10.1016/j.apcatb.2018.12.049.
[35] C.H. Choi, L. Lin, S. Gim, S. Lee, H. Kim, X. Wang, W. Choi, Polymeric carbon nitride with localized aluminum coordination sites as a durable and efficient photocatalyst for visible light utilization, Acs Catal. 8 (2018) 4241–4256, https://doi.org/10.1021/acscatal.7b03512.
[36] C. Zhou, P. Xu, C. Lai, C. Zhang, G. Zeng, D. Huang, M. Cheng, L. Hu, W. Xiong, X. Wen, L. Qin, J. Yuan, W. Wang, Rational design of graphic carbon nitride copolymers by molecular doping for visible-light-driven degradation of aqueous sulfamethazine and hydrogen evolution, Chem. Eng. J. 359 (2019) 186–196, https://doi.org/10.1016/j.cej.2018.11.140.
[37] X. Liu, X. Ma, K. Dong, K. Zheng, X. Wang, Investigating the origins of acute and long-term toxicity posed by municipal wastewater using fractionation, Environ. Technol. 41 (2019) 1–29, https://doi.org/10.1080/09593330.2019.1567602.
[38] The State Environmental Protection Administration, China, Water Quality-Determination of the acute toxicity-Luminescent bacteria test, The State Environmental Protection Administration, China, Beijing, China, 1995.
[39] T. Wu, J. Gu, C. Peng, S. Wu, H. Chen, F. Jiang, Study on photocatalytic degradation of bisphenol A in water by graphite phase carbon nitride homojunction, China Environ. Sci. 41 (2021) 3255–3265, https://doi.org/10.19674/j.cnki.issn1000-6923.20210223.006.
[40] C. Zhou, Design of polymeric carbon nitride and their performance and mechanism in catalytic degradation of antibiotic contaminants in water under visible light, Hunan University, China, 2019.
[41] G. Algara-Siller, N. Severin, S.Y. Chong, T. Björkman, R.G. Palgrave, A. Laybourn, M. Antonietti, Y.Z. Khimyak, A.V. Krasheninnikov, J.P. Rabe, U. Kaiser, A. I. Cooper, A. Thomas, M.J. Bojdys, Triazine-based graphitic carbon nitride: a two-dimensional semiconductor, Angew. Chem. 126 (2014) 7580–7585, https://doi.org/10.1002/anie.201402191.
[42] Z. Wu, Y. Zhao, X. Chen, Y. Guo, H. Wang, Y. Jin, P. He, Q. Wei, B. Wang, Preparation of polymeric carbon nitride/TiO_2 heterostructure with NH_4Cl as template: Structural and photocatalytic studies, J. Phys. Chem. Solids 164 (2022), 110629, https://doi.org/10.1016/j.jpcs.2022.110629.
[43] W. Wang, Z. Zeng, G. Zeng, C. Zhang, R. Xiao, C. Zhou, W. Xiong, Y. Yang, L. Lei, Y. Liu, D. Huang, M. Cheng, Y. Yang, Y. Fu, H. Luo, Y. Zhou, Sulfur doped carbon quantum dots loaded hollow tubular g-C_3N_4 as novel photocatalyst for destruction of Escherichia coli and tetracycline degradation under visible light, Chem. Eng. J. 378 (2019), 122132, https://doi.org/10.1016/j.cej.2019.122132.
[44] H. Gao, S. Yan, J. Wang, Z. Zou, Ion coordination significantly enhances the photocatalytic activity of graphitic-phase carbon nitride, Dalton Trans. 43 (2014) 8178–8183, https://doi.org/10.1039/C3DT53224K.
[45] Z. Chen, S. Pronkin, T.P. Fellinger, K. Kailasam, G. Vilé, D. Albani, F. Krumeich, R. Leary, J. Barnard, J.M. Thomas, J. Pérez-Ramírez, M. Antonietti, D. Dontsova, Merging single-atom-dispersed silver and carbon nitride to a joint electronic system via copolymerization with silver tricyanomethanide, Acs Nano 10 (2016) 3166–3175, https://doi.org/10.1021/acsnano.5b04210.
[46] J. Li, D. Wu, J. Iocozzia, H. Du, X. Liu, Y. Yuan, W. Zhou, Z. Li, Z. Xue, Z. Lin, Achieving efficient incorporation of π-Electrons into graphitic carbon nitride for markedly improved hydrogen generation, Angew. Chem. 131 (2019) 2007–2011, https://doi.org/10.1002/ange.201813117.
[47] Y. Ma, T. Zhang, P. Zhu, H. Cai, Y. Jin, K. Gao, J. Li, Fabrication of Ag_3PO_4/polyaniline-activated biochar photocatalyst for efficient triclosan degradation process and toxicity assessment, Sci. Total Environ. 821 (2022), 153453, https://doi.org/10.1016/j.scitotenv.2022.153453.
[48] H. Anwer, J.W. Park, Synthesis and characterization of a heterojunction rGO/ZrO_2/Ag_3PO_4 nanocomposite for degradation of organic contaminants, J. Hazard. Mater. 358 (2018) 416–426, https://doi.org/10.1016/j.jhazmat.2018.07.019.
[49] J. Wang, M. Yue, Y. Han, X. Xu, Q. Yue, S. Xu, Highly-efficient degradation of triclosan attributed to peroxymonosulfate activation by heterogeneous catalyst g-C_3N_4/$MnFe_2O_4$, Chem. Eng. J. 391 (2020), 123554, https://doi.org/10.1016/j.cej.2019.123554.
[50] A. Tiwari, A. Shukla, Lalliansanga, D. Tiwari, S.M. Lee, Synthesis and characterization of Ag^0(NPs)/TiO_2 nanocomposite: insight studies of triclosan removal from aqueous solutions, Environ. Technol. 41 (2019) 3500–3514, https://doi.org/10.1080/09593330.2019.1615127.
[51] J. Peng, C. Zhang, Y. Zhang, S. Shao, P. Wang, G. Liu, H. Dong, D. Liu, J. Shi, Z. Cao, H. Liu, S. Gao, Efficient removal of triclosan via peroxymonosulfate activated by a ppb level dosage of Co(II) in water: Reaction kinetics, mechanisms and detoxification, Ecotoxicol. Environ. Saf. 198 (2020), 110676, https://doi.org/10.1016/j.ecoenv.2020.110676.
[52] Y. Guan, J. Ma, Y. Ren, Y. Liu, J. Xiao, L. Lin, C. Zhang, Efficient degradation of atrazine by magnetic porous copper ferrite catalyzed peroxymonosulfate oxidation via the formation of hydroxyl and sulfate radicals, Water Res. 47 (2013) 5431–5438, https://doi.org/10.1016/j.watres.2013.06.023.
[53] Q. Zhang, F. Wang, Z. Xie, Y. Su, P. Chen, W. Lv, h Liu, G. Liu, Photocatalytic degradation mechanism of mefenamic acid by N-doped carbon quantum dots loaded on TiO_2, China Environ. Sci. 37 (2017) 2930–2940, https://doi.org/10.3969/j.issn.1000-6923.2017.08.015.
[54] F. Dong, Z. Wang, Y. Li, W. Ho, S.C. Lee, Immobilization of polymeric g-C_3N_4 on structured ceramic foam for efficient visible light photocatalytic air purification with real indoor illumination, Environ. Sci. Technol. 48 (2014) 10345–10353, https://doi.org/10.1021/es502290f.
[55] X. Shangguan, B. Fang, C. Xu, Y. Tan, Y. Chen, Z. Xia, W. Chen, Fabrication of direct Z-scheme $FeIn_2S_4$/Bi_2WO_6 hierarchical heterostructures with enhanced photocatalytic activity for tetracycline hydrochloride photodegradation, Ceram. Int. 47 (2021) 6318–6328, https://doi.org/10.1016/j.ceramint.2020.10.210.
[56] H. Azarpira, M. Sadani, M. Abtahi, N. Vaezi, S. Rezaei, Z. Atafar, S.M. Mohseni, M. Sarkhosh, M. Ghaderpoori, H. Keramati, R.H. Pouya, A. Akbari, V. Fanai, Photocatalytic degradation of triclosan with UV/iodide/ZnO process: performance, kinetic, degradation pathway, energy consumption and toxicology, J. Photochem. Photobiol. A 371 (2019) 423–432, https://doi.org/10.1016/j.jphotochem.2018.10.041.
[57] C. Solá-Gutiérrez, S. Schroder, M. San-Román, I. Ortiz, Critical review on the mechanistic photolytic and photocatalytic degradation of triclosan, J. Environ. Manag. 260 (2020), 110101, https://doi.org/10.1016/j.jenvman.2020.110101.
[58] V. Kosera, E. Lumbaque, A. Dallegrave, M. Gomes, V.C.S.D. Paula, A.M.D. Freitas, C. Sirtori, E.S. Chaves, E.R.L. Tiburtius, A comparison of the photolytic and photocatalytic degradation of triclosan: identification of transformation products and ecotoxicity evaluation, J. Braz. Chem. Soc. 32 (2021) 1531–1540, https://doi.org/10.21577/0103-5053.20210050.
[59] L.A. Constantin, I. Nitoi, N.I. Cristea, M.A. Constantin, Possible degradation pathways of triclosan from aqueous systems via TiO_2 assisted photocatalyis, J. Ind. Eng. Chem. 58 (2018) 155–162, https://doi.org/10.1016/j.jiec.2017.09.020.
[60] S.C. Pragada, A.K. Thalla, Polymer-based immobilized Fe_2O_3–TiO_2/PVP catalyst preparation method and the degradation of triclosan in treated greywater effluent by solar photocatalysis, J. Environ. Manag. 296 (2021), 113305, https://doi.org/10.1016/j.jenvman.2021.113305.